Photocatalytic Activation of Water and Methane over Modified Gallium Oxide for Hydrogen Production

ARTICLE *in* THE JOURNAL OF PHYSICAL CHEMISTRY C · JUNE 2010

Impact Factor: 4.77 · DOI: 10.1021/jp1012126

3 AUTHORS, INCLUDING:

Hisao Yoshida
Kyoto University
183 PUBLICATIONS **4,548** CITATIONS

SEE PROFILE

Photocatalytic Activation of Water and Methane over Modified Gallium Oxide for Hydrogen Production

Katsuya Shimura,[†] Tomoko Yoshida,[‡] and Hisao Yoshida*,[†]

Department of Applied Chemistry, Graduate School of Engineering and Division of Environmental Research, EcoTopia Science Institute, Nagoya University, Nagoya 464-8603, Japan

Received: February 8, 2010; Revised Manuscript Received: May 7, 2010

Ga_2O_3 photocatalysts showed a high and stable activity for the photocatalytic steam reforming of methane (PSRM; $2H_2O(g) + CH_4 \rightarrow 4H_2 + CO_2$) around room temperature. The activity was much influenced by the cocatalyst and the crystal structure of Ga_2O_3; the highest activity was obtained over Pt-loaded β-type Ga_2O_3 with specific surface area of $10-20\ m^2\ g^{-1}$. The addition of metal cations into the bulk and/or on the surface of Ga_2O_3 was also effective to improve the photocatalytic activity; metal cations having both a smaller oxidation number than that of Ga^{3+} and a similar ionic radius to that of Ga^{3+}, such as Mg^{2+} and Zn^{2+}, were effective as the dopant into the bulk of β-Ga_2O_3, while cations of the aluminum group such as In^{3+} and Al^{3+} were effective as the surface additives. When we compared the activity for the PSRM with those for the water decomposition (WD; $H_2O \rightarrow H_2 + {}^1/_2O_2$) and the methane decomposition (MD; $CH_4 \rightarrow x/2H_2 + CH_{4-x}$), it was revealed that the improvement of the bulk processes would mainly influence the water activation while that of the surface processes would affect the methane activation.

Introduction

Hydrogen as an environmentally benign fuel should be produced from renewable resources and natural energy to realize a sustainable society. Although water decomposition (referred to as WD; $H_2O \rightarrow H_2 + {}^1/_2O_2$, $\Delta G_{298K}^\circ = 237\ kJ\ mol^{-1}$) by using solar energy and photocatalyst would be an ideal hydrogen production method,[1−3] it is not easy to promote this reaction effectively because of a large and positive value of Gibbs free energy change (ΔG). One possible way to accelerate the formation of hydrogen is employing a sacrificial reagent, which can consume the photogenerated holes or activated oxygen species to reduce their reverse reactions. Sacrificial reagents reported so far were some kinds of carbon-related solid materials such as active carbon,[4] saccharides (i.e., sugar, starch, and cellulose),[5] coal and tar sand,[6] and some kinds of compounds such as MeOH,[7] EtOH,[8] C_2H_4[9] and CO.[10] Since some of them, such as EtOH, sugar, starch, and cellulose, could be recognized as renewable resources, it is also worthwhile to develop these photocatalytic systems.

Recently, we reported that hydrogen could be effectively produced from water by using methane as the sacrificial reagent.[11−14] In this photocatalytic system, a consumption of 2 mol of water and only 1 mol of methane gives 4 mol of hydrogen as follows

$$2H_2O(g) + CH_4 \rightarrow 4H_2 + CO_2 \qquad (1)$$

$$\Delta G_{298K}^\circ = 113\ kJ\ mol^{-1}$$

The reaction shown in eq 1 can be also interpreted as a photocatalytic steam reforming of methane, thus referred to as photocatalytic steam reforming of methane (PSRM).[11] Since methane is a main component of biogas as one of the renewable resources, the PSRM can become a desirable hydrogen production method from renewable resources and solar energy. It is expected that the PSRM would produce hydrogen more efficiently than the WD due to the low ΔG value. The PSRM also has an advantage of converting photoenergy into chemical energy.

We first discovered this reaction over the Pt/TiO_2 photocatalyst,[11,12] and then we once assumed that water activation would be the most important process to promote the PSRM effectively. Since many active photocatalysts for the WD in UV light region had been already reported by other researchers, such as La-doped $NaTaO_3$ ($NaTaO_3$:La),[15] $SrTiO_3$,[16] $CaTiO_3$,[17] $KTaO_3$,[18] and $K_4Nb_6O_{17}$,[19] we examined these photocatalysts for the PSRM and found that $NaTaO_3$:La loaded with Pt cocatalyst showed a higher activity than those of Pt/TiO_2[11,13] and $Pt/CaTiO_3$.[14] However, other photocatalysts showed very low activity for the PSRM even when Pt cocatalyst was loaded. These results imply that the photocatalyst for the PSRM must activate both water and methane simultaneously.

In the present study, we examined the photocatalytic activity of gallium oxide for the PSRM around room temperature (ca. 308 K). Ga_2O_3 with NiO cocatalyst was reported to show a high photocatalytic activity for the WD.[20,21] Ga_2O_3 photocatalyst was also reported to be active for methane activation in the photocatalytic nonoxidative coupling of methane (referred to as PCM) around room temperature[22] and the photocatalytic reduction of carbon dioxide by methane at mild temperature such as 473 K.[23] Thus, it is considered that the Ga_2O_3 photocatalyst can activate both water and methane. Therefore, the Ga_2O_3 photocatalyst is expected to show a high activity for the PSRM. We here examined some kinds of Ga_2O_3 photocatalysts with or without the addition of metal ions and cocatalyst for the PSRM. We also evaluate the activity for the hydrogen production from each reactant, water and methane, and discuss the controlling factors for their activation.

* Corresponding author, yoshidah@apchem.nagoya-u.ac.jp.
[†] Department of Applied Chemistry, Graduate School of Engineering.
[‡] Division of Environmental Research, EcoTopia Science Institute.

10.1021/jp1012126
Published on Web 06/10/2010

Experimental Methods

Preparation of Photocatalysts. Ga_2O_3 samples were commercially obtained or prepared from $Ga(NO_3)_3 \cdot 8H_2O$ (Kishida, 99.0%). Two Purchased Ga_2O_3 samples from Kojundo (Lot No. 139595 and Lot No. 188962) and one from Soekawa were employed and referred to as $Ga_2O_3(K_1)$, $Ga_2O_3(K_2)$, and $Ga_2O_3(S)$, respectively. BET specific surface areas were 4.1, 11.0, and 9.3 $m^2\ g^{-1}$, respectively. Mean crystallite sizes were 45, 27, and 30 nm, respectively. All of them had a β-type crystal phase, and their purities were 99.99%. Other Ga_2O_3 samples with different crystal phases were prepared according to the literature.[24] To obtain α-Ga_2O_3, $Ga(NO_3)_3 \cdot 8H_2O$ (10 g) was dissolved in distilled water (250 mL). Then, 10 vol % ammonia−water was added to the solution until no additional precipitation was observed. The suspension was filtered off with suction, washed with distilled water, and dried at 343 K overnight. The obtained powder was calcined in air at 823 K for 6 h. β-Ga_2O_3 was prepared by almost the same procedure as that of α-Ga_2O_3, but the calcination temperature was 973 K. γ-Ga_2O_3 was also prepared by almost the same procedure as that of α-Ga_2O_3, but EtOH was used as the solvent. To prepare δ-Ga_2O_3, $Ga(NO_3)_3 \cdot 8H_2O$ was calcined in the flow of air at 473 K for 12 h and then calcined at 773 K for 6 h in an oven. X-ray diffraction patterns confirmed that these Ga_2O_3 samples were successfully prepared to be in each desired crystal phase.

The several kinds of metal cations were examined as surface additives or bulk dopants for β-Ga_2O_3. The loading amount (x) of these cations was in the range from 0.05 to 2 mol %. The precursors of examined metal ions were as follows: Li_2CO_3 (Wako, 99.0%), $Mg(NO_3)_2 \cdot 6H_2O$ (Kishida, 99.0%), $Ca(NO_3)_2 \cdot 4H_2O$ (Kishida, 98.5%), $Zn(NO_3)_2 \cdot 6H_2O$ (Kishida, 99.0%), $Sr(NO_3)_2$ (Kishida, 98.0%), $Al(NO_3)_3 \cdot 9H_2O$ (Kishida, 98.0%), $Sc(NO_3)_3 \cdot 4H_2O$ (Mitsuwa, 99.9%), $Y(NO_3)_3 \cdot 6H_2O$ (Kishida, 99.9%), $In(NO_3)_3 \cdot 6H_2O$ (Kishida, 98.0%), $La(NO_3)_3 \cdot 6H_2O$ (Aldrich, 99.9%), $Ce(NO_3)_3 \cdot 6H_2O$ (Kishida, 98.0%), $(NH_4)_2[TiO(C_2O_4)_2] \cdot nH_2O$ (Kishida, Chemical grade), $ZrO(NO_3)_2 \cdot 2H_2O$ (Kishida, 99.0%) and NH_4VO_3 (Kishida, 99.0%). The metal cation was added by the following procedures: The purchased β-Ga_2O_3 (2 g) was dispersed into an aqueous solution (50 mL) of the precursor and stirred for 0.5 h, followed by evaporation to dryness with a rotary evaporator. Then the obtained powder was dried in an oven at 333 K overnight and calcined in air typically at 773 or 1273 K for 6 h. When calcined at 773 K, the metal ions were expected to be deposited as metal oxide particles or dispersed oxide species on the surface of β-Ga_2O_3, thus referred to as $MO_y(x)/Ga_2O_3$. On the other hand, when calcined at 1273 K, they were expected to form composites with β-Ga_2O_3, thus referred to as Ga_2O_3:M(x).

The doped and undoped Ga_2O_3 samples were loaded with metals (Pt, Rh, Au, Pd, and Ni) as cocatalyst. The loading amount (z) of these metals was in the range from 0.01 to 0.1 wt %. The employed precursors were as follows: $Pt(NO_2)_2(NH_3)_2$ aqueous solution (Tanaka kikinzoku, 4.533 wt % as Pt), $Rh(NO_3)_3$ aqueous solution (Tanaka kikinzoku, 4.282 wt % as Rh), $HAuCl_4$ (Kishida, 99%), $PdCl_2$ (Kishida, 99%), and $Ni(NO_3)_2 \cdot 6H_2O$ (Wako, 98%). Metal cocatalysts were loaded by an impregnation method. The Ga_2O_3 sample (2 g) was dispersed into an aqueous solution (50 mL) of the metal precursor and stirred for 0.5 h, followed by evaporation to dryness with a rotary evaporator. Then, the obtained powder was dried in an oven at 333 K overnight. When we used these samples without further pretreatment before the photocatalytic reaction test, the metal precursors adsorbed on Ga_2O_3 should be reduced during the photoirradiation in the flow of water and methane (in situ photodeposition) as reported in the previous study.[12] An oxidative pretreatment was carried out in air at 773 K for 2 h. A reductive pretreatment was carried out in the flow of hydrogen at 473 K for 0.5 h after the oxidative pretreatment. The sample with the cocatalyst was referred to as $Pt(z)/Ga_2O_3$ for example.

MgO, ZnO, Ga_2O_3, $ZnGa_2O_4$, and $MgGa_2O_4$ were used as the reference samples for XAFS analysis. MgO (JRC-MGO-1) was supplied from the Catalyst Society of Japan and it was calcined in air at 773 K for 1 h before the measurement of XAFS. ZnO and Ga_2O_3 were commercially obtained (Kojundo, 99.99%). $ZnGa_2O_4$ was prepared by a solid-state reaction method. ZnO and Ga_2O_3 were physically mixed by a wet ball-milling method with acetone at room temperature (120 rpm, 24 h) and calcined in air at 1473 K for 20 h. $MgGa_2O_4$ was prepared by almost the same procedure as that of $ZnGa_2O_4$, but the calcination temperature was 1573 K. X-ray diffraction revealed that $ZnGa_2O_4$ and $MgGa_2O_4$ were obtained although very small diffractions corresponding to β-Ga_2O_3 were also detected in the $MgGa_2O_4$ sample.

Photocatalytic Reaction Tests. The reaction tests were carried out with a fixed-bed flow reactor in a way similar to the previous studies.[11−14] The catalysts were granulated to a size of 400−600 μm. The quartz cell ($60 \times 20 \times 1$ mm^3) was filled with the mixture of the catalyst (0.8 g) and quartz granules (0.7 g). Prior to the photoreaction test, to clean the catalyst surface, the catalyst was photoirradiated by a 300 W xenon lamp in a flow of water vapor (3%) with Ar carrier. Water vapor was introduced by the carrier gas from a bubbling saturator containing distilled water at room temperature. When the reaction was carried out in the flow of methane, the reactor was further heated at 423 K for 1 h in the flow of Ar to remove the adsorbed water before the reaction. Then the reaction gas, a mixture of H_2O vapor and/or CH_4 with Ar carrier, was introduced into the quartz cell at the flow rate of 50 mL min^{-1}, and the reaction was carried out without heating at atmospheric pressure upon photoirradiation with the 300 W xenon lamp. The concentration of water vapor and methane was 1.5% (30 μmol min^{-1}) and 50% (1020 μmol min^{-1}), respectively, and the light of the entire wavelength region from the xenon lamp was irradiated without passing any filters, where the light intensity measured in the range of 230−280 and 310−400 nm were ca. 14 and 60 mW cm^{-2}, respectively. The temperature of the reaction cell increased to ca. 308 K during the photoirradiation. The outlet gas was analyzed by online gas chromatography with a thermal conductivity detector. Hydrogen production rates in the flow of water and in the flowing mixture of water and methane shown in each figure and table were taken from the value of the steady state, while those in the flow of methane were the value at 5 h after the reaction started.

Apparent quantum yield around 254 nm (Φ) on Pt/Ga_2O_3 was calculated from a result of the reaction experiment by using an optical band-pass filter permitting only the light around 254 ± 20 nm (Ashahi spectra). The incident light intensity measured in the range of 254 ± 20 nm was 7.3 mW cm^{-2}. The photoirradiated area was limited to 6 cm^2. The reaction gas was a mixture of H_2O vapor (1.5%) and CH_4 (50%) with Ar carrier. The total flow rate was 50 mL min^{-1}. The Φ was calculated by the following equation: $\Phi(\%) = N_e/N_p \times 100$, where N_e was the number of reacted electrons upon photoirradiation and N_p was the number of incident photons. The number of reacted electrons was determined from the hydrogen production rate, assuming that two electrons produced one hydrogen molecule ($2H^+ + 2e^- \rightarrow H_2$). The number of incident photons was

TABLE 1: Effect of Pt Loading and Its Amount on the Hydrogen Production Rate over the β-Ga_2O_3 Photocatalysts in the Flow of Various Reactants[a]

entry	Pt loading amount/wt %	hydrogen production rate/μmol min^{-1} (a) $H_2O + CH_4$	(b) H_2O	(c) CH_4
1	0.00	0.15	0.02	0.01
2	0.01	0.51	0.15	0.15
3	0.02	0.58	0.08	0.14
4	0.03	0.57	0.05	0.15
5	0.05	0.55	0.02	0.16

[a] The Ga_2O_3(S) sample was used. Pt was loaded by the impregnation method using $Pt(NO_2)_2(NH_3)_2$, followed by calcination at 773 K.

determined from the value measured by a Si photodiode (Topcon UVR-2 with UD-25).

Characterizations of Photocatalysts. Powder X-ray diffraction (XRD) patterns were recorded at room temperature on a Rigaku diffractometer RINT 2500 using Ni-filtered Cu Kα radiation (50 kV, 100 mA). The mean crystallite sizes of the β-Ga_2O_3 samples were estimated from the diffraction line at 35.2°. The diffuse reflectance (DR) UV−visible spectrum was recorded at room temperature on a JASCO V-570 equipped with an integrating sphere covered with $BaSO_4$. $BaSO_4$ was used as the reference. The Brunauer−Emmett−Teller (BET) specific surface area of the sample was calculated from the amount of N_2 adsorption at 77 K, which was measured by a Quantachrome Monosorb. Mg K-edge XANES spectra of Mg-modified Ga_2O_3 samples and reference samples (MgO, $MgGa_2O_4$ and β-Ga_2O_3) were measured at the BL-1A station of the UVSOR, Institute for Molecular Science, Okazaki, Japan. The spectra were recorded in a total electron yield mode at room temperature with a beryl two-crystal monochromator. The powder sample was put on the first dynode of the electron multiplier with carbon adhesive tape. Zn K-edge XAFS spectra of Zn-modified Ga_2O_3 samples and reference samples (ZnO and $ZnGa_2O_4$) were recorded at the NW-10A station[25] of KEK-PF (Photon Factory, Institute of Materials Structure Science, High Energy Accelerator Research Organization) at room temperature with a Si(311) double crystal monochromator in a transmission mode. The samples were packed in each polyethylene film cell in air. The spectra were analyzed with REX 2000 software (Rigaku). Fourier transform of Zn K-edge EXAFS was performed in the range of ca. 3−12 Å^{-1} after background subtraction. The inverse Fourier transform was carried out in the range of ca. 2.5−3.5 Å. The empirical parameters for Zn−Zn and Zn−Ga shells were extracted from the second coordination peak in the spectra of ZnO and $ZnGa_2O_4$, respectively, and used for the curve fitting analysis. The ratio of the tetrahedrally coordinated GaO_4 species to the octahedrally coordinated GaO_6 species (T_d/O_h) was obtained from the Ga K-edge XANES analysis of the Ga_2O_3 samples, according to a previous study.[26]

Results and Discussion

Effect of Metal Cocatalyst on Photocatalytic Activities of Ga_2O_3. Table 1 shows the hydrogen production rate over β-Ga_2O_3 photocatalysts with or without Pt cocatalyst. When β-Ga_2O_3 without metal loading was photoirradiated in the flow of water vapor (Table 1, entry 1b), a small amount of hydrogen was continuously produced by water decomposition (WD; $H_2O \rightarrow H_2 + {}^1/_2O_2$) as reported.[20] In the flow of methane (Table 1, entry 1c), hydrogen and ethane were produced constantly, where photocatalytically nonoxidative coupling of methane (PCM; $CH_4 \rightarrow H_2 + C_2H_6$) occurred as reported.[22] In the flowing mixture of water vapor and methane (Table 1, entry 1a), the hydrogen production rate was clearly higher than the sum of the values in the flow of each reactant only, i.e., water or methane. Carbon dioxide was also observed under the quantitation limit, but oxygen was not observed. These imply that the PSRM (eq 1) would occur over the β-Ga_2O_3 photocatalyst.

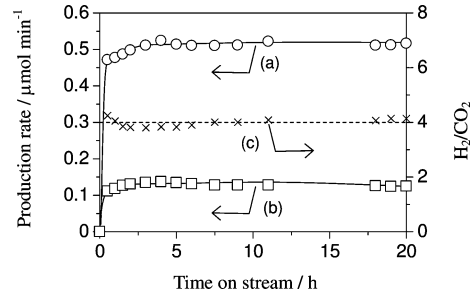

Figure 1. Time course of the production rate of (a) H_2 and (b) CO_2 on the Pt(0.01)/β-Ga_2O_3 sample and (c) that of molar ratio of the produced H_2 to CO_2 in the flowing mixture of water vapor and methane. The Ga_2O_3(S) sample was used. Pt was loaded by the impregnation method, followed by calcination at 773 K.

Pt-loaded samples prepared by the impregnation method followed by calcination at 773 K exhibited higher hydrogen production rates in each reaction condition than the bare sample did (Table 1, entries 2−5). Figure 1 shows the time course of the production rate of hydrogen and carbon dioxide, as well as the molar ratio of hydrogen to carbon dioxide (H_2/CO_2), over the Pt(0.01)/β-Ga_2O_3 sample in the flowing mixture of water vapor and methane. The induction period was quite short as compared with Pt/TiO_2[12] and Pt/$NaTaO_3$:La photocatalysts.[13] The activity was constant at least for 20 h, and the molar ratio of hydrogen to carbon dioxide was constant at 4. Production of byproducts such as oxygen and carbon monoxide was not observed. These facts show that all of the reacted water and methane molecules would convert into hydrogen and carbon dioxide. In other words, it could be said that hydrogen was equally produced from water and methane. If we assumed that Pt would be the active sites for the hydrogen production via reaction between proton and photoexcited electron ($2H^+ + 2e^- \rightarrow H_2$), the turnover frequency per loaded Pt atom was calculated to be 75 h^{-1} for Pt(0.01)/β-Ga_2O_3. The reaction did not proceed in the dark or without photocatalyst. These results suggest that the PSRM would proceed photocatalytically over the Pt/β-Ga_2O_3 samples. The apparent quantum yield in the range of 254 ± 20 nm at a light intensity of 7.3 mW cm^{-2} was estimated to be 7.9%. The activity of other Pt/β-Ga_2O_3 photocatalysts was also constant for a long time, which was a similar result as shown in Figure 1. The activity of these Pt/β-Ga_2O_3 catalysts without further modification corresponded to about one-third activity of Pt/$NaTaO_3$:La photocatalyst that was the highest activity for this reaction so far. However, since Ga_2O_3 photocatalysts showed high photocatalytic activities for both the WD and the PCM as well as the PSRM, we can investigate the details of the photocatalyst for the PSRM through the activity tests of the Ga_2O_3 photocatalyst for each reactant.

When Pt loading amount increased from 0.01 to 0.05 wt %, the activity for the PSRM in the flow of water and methane first increased and then slightly decreased as shown in Table 1 entries 2a−5a; the highest activity was obtained over Pt(0.02)/β-Ga_2O_3 among them (entry 3a). In the flow of water vapor the activity for the WD largely decreased with the increase of Pt loading amount (entries 2b−5b). On the other hand, in the flow of methane the hydrogen production rate over these Pt-loaded

TABLE 2: Effect of Metal Cocatalyst on the Hydrogen Production Rate in the Flow of Various Reactants[a]

	hydrogen production rate/μmol min^{-1}		
photocatalyst	(a) $H_2O + CH_4$	(b) H_2O	(c) CH_4
Ga_2O_3	0.15	0.02	0.01
Pt(0.01)/Ga_2O_3	0.51	0.15	0.15
Rh(0.01)/Ga_2O_3	0.45	0.17	0.13
Au(0.01)/Ga_2O_3	0.24	0.02	0.02
Pd(0.01)/Ga_2O_3	0.20	0.04	0.04
Ni(0.01)/Ga_2O_3	0.07	0.01	trace

[a] The Ga_2O_3(S) sample was used except for the Ni-loaded sample. In the Ni-loaded sample, the $Ga_2O_3(K_1)$ was used. Pt was loaded by the impregnation method, followed by calcination at 773 K. Rh was loaded by the impregnation method, followed by calcination at 773 K and the hydrogen reduction at 473 K. Au, Pd, and Ni were loaded by the impregnation method and reduced by the in situ photodeposition.

TABLE 3: Effect of Crystal Phase on the Hydrogen Production Rate over the Pt(0.05)/Ga_2O_3 Photocatalysts in the Flow of Various Reactants

				hydrogen production rate/μmol min^{-1}		
crystal phase[a]	SA[b]/m^2 g^{-1}	BG[c]/eV	T_d/O_h[d]	(a) $H_2O + CH_4$	(b) H_2O	(c) CH_4
α	32.6	4.7	0.20	0.39	0.03	0.10
β	18.7	4.7	0.92	0.57	0.02	0.20
γ	109.4	4.4	0.83	0.50	0.01	0.15
δ	80.8	4.3	0.76	0.31	0.01	0.05

[a] The Ga_2O_3 samples were prepared from $Ga(NO_3)_3 \cdot 8H_2O$. Pt was loaded by the impregnation method, followed by calcination at 773 K. [b] SA, BET specific surface area. [c] BG, band gap. [d] T_d/O_h, ratio of the tetrahedrally coordinated Ga species to the octahedrally coordinated Ga species, which was obtained from the Ga K-edge XAFS analysis of the Ga_2O_3 samples.

Ga_2O_3 samples was almost similar (entries 2c−5c), where ethane was hardly produced unlike over the none-loaded β-Ga_2O_3 sample. The activity of these Pt-loaded photocatalysts slowly decreased as the reaction continued. For example, hydrogen production rate over the Pt(0.01)/Ga_2O_3 in the flow of methane decreased from 0.17 to 0.15 μmol min^{-1} while the photocatalytic reaction continued for 5 h. Their color after the photocatalytic reaction in the flow of methane had changed to pale yellow. These results suggest that methane decomposition (referred to as MD; $CH_4 \rightarrow CH_{4-x} + {}^1/_2xH_2$) and the successive oligomerization would mainly occur over the metal-loaded Ga_2O_3 samples in the flow of methane. The decrease of the WD activity with increasing Pt loading amount would be due to the promotion of the reverse reaction between produced hydrogen and oxygen to form water by Pt catalyst.[27] However, loading a large amount of Pt did not drastically decrease the activities for the PSRM in the flowing mixture of water and methane and the MD in the flow of methane. This indicates that contribution of Pt to the reverse reaction for the PSRM and the MD would be much smaller. On the other hand, hydrogen production rate of the PSRM was much higher than that of the WD and the MD in all Ga_2O_3 samples (see also Tables 2, 3, 5, and 6, and Figure 4). This shows that activated water and methane species would promote the decomposition of another molecule or these species would suppress the reverse reaction of the WD and the MD.

Other metals were also examined as a cocatalyst for the β-Ga_2O_3 photocatalyst. Figure 2 shows the hydrogen production rate in the flowing mixture of water vapor and methane over the M(0.01)/β-Ga_2O_3 samples prepared by the different method

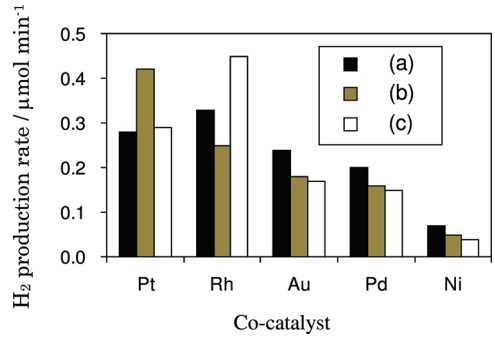

Figure 2. Effect of the loading method on the PSRM activity of the M(0.01)/β-Ga_2O_3 samples. The metals were loaded by the impregnation method followed by (a) the in situ photodeposition, (b) calcination at 773 K, and (c) calcination at 773 K and successive hydrogen reduction at 473 K. The Ga_2O_3(S) sample was used for Rh-, Au-, and Pd-loaded sample. In Pt- and Ni-loaded samples, the $Ga_2O_3(K_1)$ sample was used.

and successive treatment. Among the Pt-loaded samples, the highest activity was obtained over the catalyst prepared by the impregnation method followed by calcination in air. Among the Rh-loaded samples, the catalyst prepared by the impregnation method followed by calcination in air and successive hydrogen reduction showed the highest activity. In the Au-, Pd-, and Ni-loaded samples, the hydrogen production rate became the highest value when the cocatalyst was loaded by the impregnation method and the successive in situ photodeposition. Among these photocatalysts listed here, the high activity was obtained over the Pt- or Rh-loaded photocatalysts. Since these metals had a comparatively large work function, 5.7 and 5.0 eV, respectively,[28] the rapid separation of photoexcited electrons and holes could be expected, which would provide the high activity.

To know their activities for each reactant, i.e., water and methane, reaction tests were carried out in the flow of either water or methane. Table 2 shows the hydrogen production rate over the M(0.01)/β-Ga_2O_3 samples prepared by the most suitable loading method. When any metal cocatalyst was loaded on the β-Ga_2O_3 sample, the hydrogen production rate increased in all kinds of reactions, except for the Ni-loaded photocatalyst. In Table 2, the order of the activity for the PSRM in the flowing mixture of water and methane (Pt > Rh > Au > Pd > Ni) was similar with that for the WD in the flow of water (Rh > Pt > Pd > Au > Ni) and that for the MD in the flow of methane (Pt > Rh > Pd > Au > Ni). This result shows that these metal cocatalysts could similarly contribute to the activation of both water and methane.

Influence of the Crystal Structure of Ga_2O_3. The activity of the Ga_2O_3 photocatalysts was varied with the crystal structure. Figure 3 shows the time course of the hydrogen production rate over the Pt/Ga_2O_3 samples with different crystal phase. When the reaction was carried out in a flowing mixture of water vapor and methane, the PSRM proceeded and the molar ratio of produced H_2 to CO_2 was almost 4 at steady state in all the Ga_2O_3 samples. The hydrogen production rate became constant soon over the Pt/α-Ga_2O_3 and Pt/β-Ga_2O_3 samples upon photoirradiation after a short induction period (Figure 3, curves a and b). On the other hand, the production rate on the Pt/γ-Ga_2O_3 and Pt/δ-Ga_2O_3 samples was low soon after the photoirradiation started (Figure 3, curves c and d) but gradually increased to become each steady state. Moreover, the color of the Pt/γ-Ga_2O_3 sample changed to pale brown after the reaction. As reported in the previous study on the Pt/TiO_2 photocatalyst,[12] surface organic intermediates were produced during the PSRM and the moderate accumulation of them could largely increase the

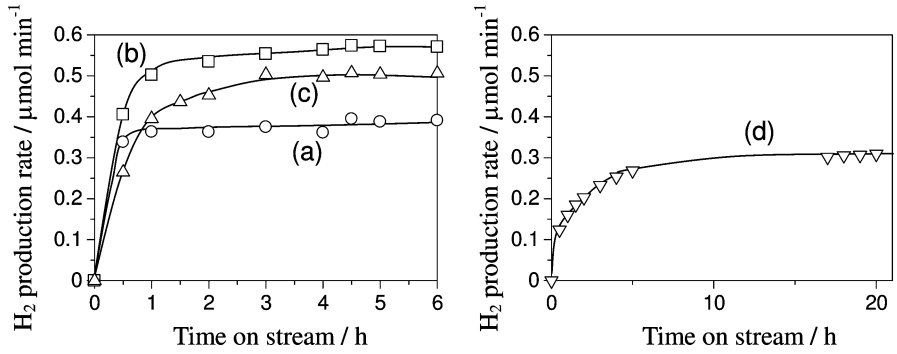

Figure 3. Time course of the hydrogen production rate in the flowing mixture of water vapor and methane over the Pt(0.05)/Ga_2O_3 samples with different crystal structures: (a) α-Ga_2O_3, (b) β-Ga_2O_3, (c) γ-Ga_2O_3, and (d) δ-Ga_2O_3. Pt was loaded by the impregnation method, followed by calcination at 773 K.

activity. This enhancement was also observed over the Pt/$NaTaO_3$:La photocatalyst.[13] Therefore, the color change over the Pt/γ-Ga_2O_3 sample would be concerned with the formation of the surface reaction intermediates. Since the production rate of the intermediates would be faster than the decomposition rate of them on the surface of the Pt/γ-Ga_2O_3 sample, a large amount of the reaction intermediates would accumulate on the surface and changed the catalyst color. On the other hand, the induction period of the Pt/δ-Ga_2O_3 sample was especially long and it continued for more than 10 h (Figure 3d). On the surface of the Pt/δ-Ga_2O_3 sample, production rate of the intermediates would be almost equal to the decomposition rate. Thus, the amount of the surface intermediates very slowly increased as the photoirradiation continued and the catalyst color did not change during the reaction. The different time profile of the four Ga_2O_3 polymorphs may be influenced by the surface structure of each Ga_2O_3 sample.

Table 3 shows the characterization results and the hydrogen production rate at steady state over the Pt/Ga_2O_3 samples with the four Ga_2O_3 polymorphs. The loading amount of Pt was 0.05 wt % in all the Ga_2O_3 samples. The order of the production rate at steady state in the flowing mixture of water vapor and methane was as follows: $\beta > \gamma > \alpha > \delta$. This was not coincident with the orders of the BET specific surface area ($\gamma > \delta > \alpha > \beta$), the band gap energy ($\alpha = \beta > \gamma > \delta$), or the ratio of the tetrahedrally coordinated GaO_4 species to the octahedrally coordinated GaO_6 species ($\beta > \gamma > \delta > \alpha$). Therefore, these factors would not be the determining factor for the activity in the PSRM although each of them would influence the activity for the PSRM to a greater or lesser extent. On the other hand, although the order of the activity for the PSRM in the flow of both water vapor and methane ($\beta > \gamma > \alpha > \delta$) was different from that for the WD in the flow of water vapor ($\alpha > \beta > \gamma = \delta$), it was the same as that for the MD in the flow of methane ($\beta > \gamma > \alpha > \delta$). This suggests that the activity of these Ga_2O_3 photocatalysts for the PSRM is much influenced by the steps concerning with the methane activation, such as adsorption of methane or activation of the C−H bond on the surface. Variation of the surface structure of Ga_2O_3 originating from the crystal structure would give the various photocatalytic properties for the methane activation and the induction period.

Influence of the Surface Area of β-Ga_2O_3. The effect of the specific surface area of the Pt/β-Ga_2O_3 samples on the activity for each reaction was examined. Four kinds of the β-Ga_2O_3 samples, $Ga_2O_3(K_1)$, $Ga_2O_3(S)$, $Ga_2O_3(K_2)$, and prepared β-Ga_2O_3, were employed. BET specific surface areas of these samples were 4.1, 9.3, 11.0, and 18.7 $m^2\ g^{-1}$, and the crystallite size were 45, 30, 27, and 25 nm, respectively, as described in the Experimental Section. When the loading amount

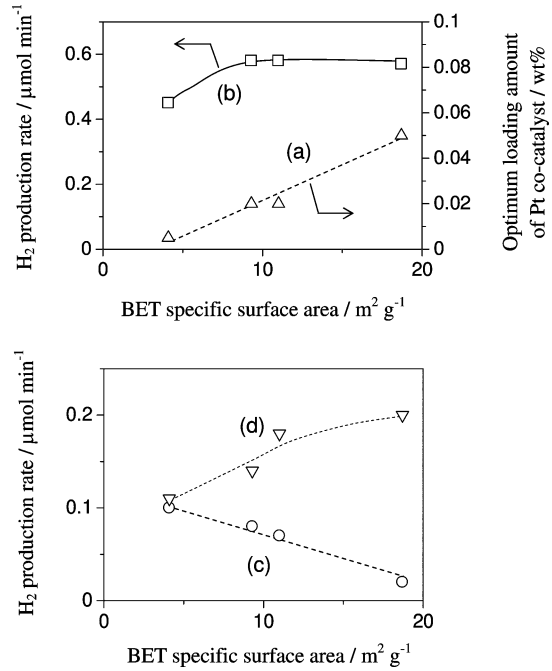

Figure 4. Effect of the BET specific surface area of the β-Ga_2O_3 samples (a) on the optimum loading amount of Pt in the PSRM and on the hydrogen production rate (b) in the flow of both water vapor and methane (the PSRM), (c) in the flow of water vapor (the WD), and (d) in the flow of methane (the MD). The β-Ga_2O_3 samples were commercially obtained or prepared from $Ga(NO_3)_3 \cdot 8H_2O$. Pt was loaded by the impregnation method, followed by calcination at 773 K.

of Pt was optimized for the PSRM on each photocatalyst, the optimum amount increased with an increase of the specific surface area (Figure 4a). The hydrogen production rate in the PSRM on the samples of the optimized Pt amount first increased with the increase of the specific surface area until 10 $m^2\ g^{-1}$ and then became constant with further increase (Figure 4b), which was different from the result of the Pt/TiO_2 photocatalyst where the PSRM activity increased with increasing the specific surface area of the Pt/TiO_2 photocatalyst in the entire range of 50−300 $m^2\ g^{-1}$.[12] On the other hand, with the increase of the specific surface area the hydrogen production rate in the WD decreased (Figure 4c) and the one in the MD increased (Figure 4d).

Here, to discuss the reaction process we assume that the whole reaction process could be roughly divided into two processes; one was the photogeneration of electrons and holes in the bulk of Ga_2O_3, followed by the migration of them to the surface, i.e., *the bulk process*, and the other was the reaction between these carriers and the reactants on the surface, i.e., *the surface*

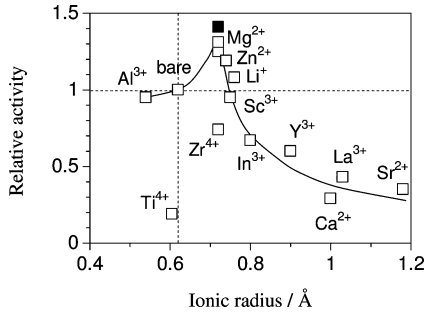

Figure 5. Relative activity of the Pt(0.01)/β-Ga_2O_3:M(2) and Pt(0.01)/β-Ga_2O_3:Mg(1) samples to the Pt(0.01)/β-Ga_2O_3 sample for the PSRM plotted vs ionic radius of each doping metal ion (M). The filled square shows the value of the Pt(0.01)/β-Ga_2O_3:Mg(1) sample. The Ga_2O_3(S) and Ga_2O_3(K_1) samples were used. Pt was loaded by the impregnation method, followed by calcination at 773 K.

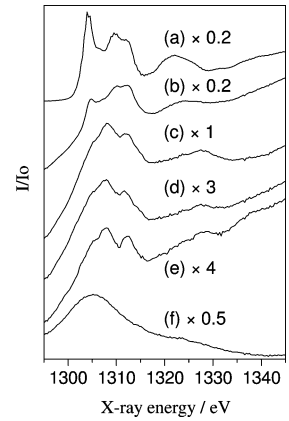

Figure 6. X-ray absorption spectra of (a) MgO, (b−d) the Mg (2 mol %)-loaded β-Ga_2O_3 samples, (e) $MgGa_2O_4$, and (f) β-Ga_2O_3. The calcination temperature was (b) 773, (c) 1073, and (d) 1273 K.

process. In the present case, with the increase of the specific surface area, the crystallite size of the photocatalyst was confirmed to decrease. Since the activity for the WD decreased with the decrease of the crystallite size of the photocatalyst, it was considered that the reaction rate for the water activation would be mainly determined by the bulk process. The decrease of the crystallite size would cause the increase of defect structures such as the grain boundary and promote the recombination of photoexcited carriers. On the other hand, two possible reasons are suggested for increasing the activity for the MD with the increase of BET specific surface area. One is that the adsorption and reaction sites of each reactant would increase with the increase of the surface. The other is that migration length of photogenerated carriers to the surface would decrease, which may be effective for the smooth migration of photoproduced carriers. However, from the result of the WD (Figure 4c), the latter possibility could not be considered. Therefore, it is reasonable that the activity for the MD would be determined by the surface process. In the case of the PSRM, since the activation of both water and methane would be necessary, there would be the optimum value of the specific surface area. In the present case, it would be around 10−20 m^2 g^{-1} (Figure 4b).

Doping Effect of Metal Ion. The addition of metal ions was examined to increase the activity of the Pt/β-Ga_2O_3 photocatalysts. Doping metal ions into the bulk of β-Ga_2O_3 was carried out by the impregnation method, followed by calcination at 1273 K (Ga_2O_3:M), where the doping amount was 2 mol %. Then Pt cocatalyst (0.01 wt %) was loaded on the doped sample. Figure 5 shows their activities for the PSRM, which were plotted against the ionic radius of the metal ions. The activity for the PSRM increased when Mg^{2+}, Zn^{2+}, or Li^+ was added. These metal ions had a similar ionic radius with that of Ga^{3+} (0.62 Å). Among the metal ions having a similar ionic radius from Al^{3+} to Li^+ (0.54−0.76 Å), the addition of Al^{3+}, Ti^{4+}, Zr^{4+}, or Sc^{3+} decreased the photocatalytic activity, while that of Mg^{2+}, Zn^{2+}, or Li^+ increased the activity. This result indicates that the metal ion having a smaller oxidation number than that of Ga^{3+} would be effective in increasing the activity for the PSRM. When the effect of doping amount was also examined in the range of 0.1−2 mol % for the Mg-doped catalyst, the highest activity was obtained over the 1 mol % doped catalyst (Figure 5, closed symbol), which showed 1.4 times higher activity than that the undoped Pt/β-Ga_2O_3 (bare sample). Therefore, it is concluded that the activity for the PSRM can be increased by doping a suitable amount of metal ions having a smaller oxidation number than that of Ga^{3+} and a similar ionic radius to that of Ga^{3+}. The radius of the metal ions introduced in the bulk would influence the crystal structure of β-Ga_2O_3. Metal ions having a similar ionic radius with that of Ga^{3+} are expected not to distort the crystal structure when they substitute for Ga^{3+} and not to give a negative effect for the activity. On the other hand, the oxidation number of the dopant cation would influence the electron density in the crystal, which might increase the photocatalytic activity. Influence of the oxidation number of the dopant on photocatalysis has been investigated by many researchers. In the WD using Pt/TiO_2[29] and $NiO/NaTaO_3$,[30,31] metal ions with a larger oxidation number than that of the substituted element were effective as the dopant. In the WD using $NiO/KTaO_3$,[18] RuO_2/GaN,[32] and Rh−Cr/$SrTiO_3$,[33] metal ions with a smaller oxidation number than that of the substituted element were effective. In the WD using Ni/β-Ga_2O_3,[21] only Zn-doped catalyst showed extremely high activity and the oxidation number of dopant cation was not correlated with the activity. In the present study, in the PSRM using Pt/Ga_2O_3, metal ions with a smaller oxidation number were effective as the dopant. These facts suggest that the optimum oxidation number of the dopant would be determined by not only the kind of the semiconductor but also the kinds of the cocatalyst and the reaction.

When the several kinds of the doped samples were characterized by DR UV−vis, XRD, and N_2 adsorption, no clear differences were observed between the doped and undoped β-Ga_2O_3 samples, which was probably due to the low doping amount. However, clear differences were observed by XAFS analysis. The states of Mg^{2+} and Zn^{2+}, both of which enhanced the activity of β-Ga_2O_3 for the PSRM, were investigated with XAFS. Figure 6 shows the X-ray absorption spectra of the Mg-loaded β-Ga_2O_3 samples and the reference samples. The MgO sample showed a Mg K-edge XANES and the β-Ga_2O_3 sample showed a Ga L_I-edge XANES (Figure 6, curves a and f), since Mg K-edge and Ga L_I-edge are at 1303 and 1301 eV, respectively. Mg K-edge XANES spectrum of the MgO sample showed some peaks at 1304, 1310, and 1322 eV and Ga L_I-edge XANES of the Ga_2O_3 sample was a broad spectrum around 1306 eV. In the spectrum of the $MgGa_2O_4$ sample (Figure 6e), the absorptions of both Mg K-edge and Ga L_I-edge should be overlapped. The spectra of the Mg^{2+}-loaded Ga_2O_3 samples calcined at various temperatures were much different from each other (Figure 6, curves b−d). For the sample calcined at 773 K (Figure 6b), the spectrum was similar to that of the MgO sample (Figure 6a). When the sample was calcined at 1073 and 1273 K (Figure 6, curves c and d), the spectra were the same as that

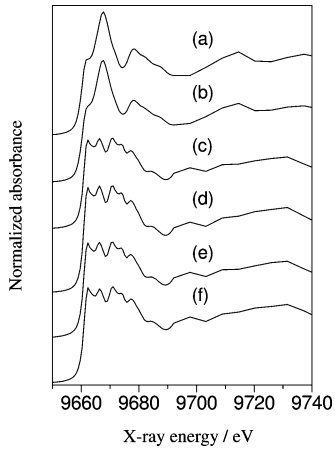

Figure 7. Zn K-edge XANES spectra of (a) ZnO, (b−e) the Zn (2 mol %)-loaded β-Ga_2O_3 samples, and (f) $ZnGa_2O_4$. The calcination temperature was (b) 773, (c) 1073, (d) 1273, and (e) 1473 K.

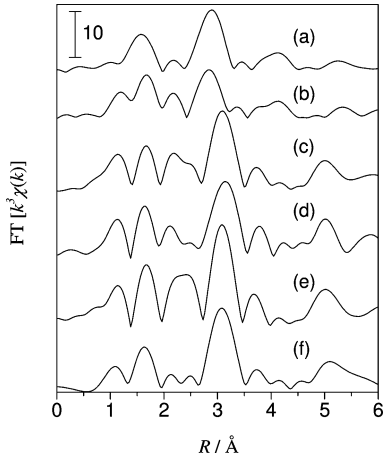

Figure 8. Fourier transforms of Zn K-edge EXAFS spectra for (a) ZnO, (b−e) the Zn (2 mol %)-loaded β-Ga_2O_3 samples, and (f) $ZnGa_2O_4$. Calcination temperature was (b) 773, (c) 1073, (d) 1273, and (e) 1473 K.

of the $MgGa_2O_4$ spinel (Figure 6e). It is suggested that the Mg ions would form a $MgGa_2O_4$ spinel-like local structure by substituting for the Ga ions at the tetrahedral site when calcined at 1073 K and higher temperatures. The same tendency was also observed over Zn K-edge XANES spectra of the Zn-loaded β-Ga_2O_3 samples, as shown in Figure 7. The spectrum of the sample calcined at 773 K (Figure 7b) was almost the same as that of the ZnO sample (Figure 7a). When the calcination temperature increased to 1073 K and higher temperatures (Figure 7c−e), the spectrum became almost the same as that of the $ZnGa_2O_4$ spinel (Figure 7f). These results suggest that the metal ions would exist in the metal oxide particles on the surface of the Ga_2O_3 when the calcination temperature was 773 K, while the sample calcined at 1073 K and higher temperatures, it would have a local structure like the spinel as the result of solid−solid reaction with the Ga_2O_3. As is the case of the Mg ions mentioned above, the Zn ions would also substitute for the tetrahedrally coordinated Ga site in the bulk of β-Ga_2O_3.

The local structure of the Zn ions added to the β-Ga_2O_3 was further examined with EXAFS in detail. Figure 8 shows the Fourier transforms of Zn K-edge EXAFS spectra for the Zn-loaded β-Ga_2O_3 samples and the reference samples. The analysis of the first coordination peak around 1.2−1.9 Å, which would correspond to the Zn−O shell, would be difficult to clarify the details for substitution, since the atomic distance between Zn and O in the ZnO (1.98 Å) and $ZnGa_2O_4$ (1.98 Å) samples and that between Ga and O in the β-Ga_2O_3 sample (1.8−2.0 Å) were very close to each other. On the other hand, the second coordination sphere around 2.5−3.5 Å, which would correspond to the Zn metal shell, provided clear evidence through the curve fitting analysis with the empirical parameters extracted from the second coordination peak for the Zn−Zn and Zn−Ga shells in the spectra of the ZnO and $ZnGa_2O_4$ samples, respectively, as shown in Table 4. The second coordination peak for the Zn-loaded β-Ga_2O_3 calcined at 773 K was only composed of the Zn−Zn shell and the length was almost the same as that of the Zn−Zn shell in the ZnO sample (3.22 Å). On the other hand, for the sample calcined at 1073 K and higher temperatures, it was only composed of the Zn−Ga shell and the length was the same as that of the Zn−Ga shell in the $ZnGa_2O_4$ sample (3.46 Å). It is concluded that the Zn ions would exist on the surface as metal oxide without mixing with the Ga_2O_3 when calcined at 773 K, and when calcined at 1073 K and higher temperatures, they would react with the Ga_2O_3 to form the spinel $ZnGa_2O_4$ partially or substitute Ga ion in the β-Ga_2O_3 having a spinel-like local structure. The small amounts of composites in semiconductor photocatalysts might show a positive effect for the activity. For example, in the famous TiO_2 sample, P-25 (Degussa) is composed of anatase TiO_2 (major, band gap 3.2 eV) and rutile TiO_2 (minor, band gap 3.0 eV), and it was proposed that the existence of small amounts of rutile TiO_2 would promote the separation of photoexcited carriers and increase the photocatalytic activity.[34,35] The same phenomenon might be seen in the present case, since the band gap of $ZnGa_2O_4$ (4.3 eV)[36] and $MgGa_2O_4$ (4.55 eV)[37] was a little smaller than that of β-Ga_2O_3 (4.7 eV). The influence of the dopant on the electron density would be still another possibility as mentioned above.

TABLE 4: Fitting Analysis for the Second Coordination Peak of Zn K-edge EXAFS Spectra

sample	calcination temperature/K	Zn−Zn N^a	Zn−Zn R^b/Å	Zn−Ga N^a	Zn−Ga R^b/Å	Debye−Waller factor ($\Delta\sigma$)
ZnO[c]		12.0	3.22			0.060
$ZnGa_2O_4$[d]				12.0	3.46	0.060
Zn-loaded Ga_2O_3[e]	773	7.7	3.20	0.0		0.050
Zn-loaded Ga_2O_3[e]	1073	0.0		10.8	3.47	0.055
Zn-loaded Ga_2O_3[e]	1273	0.0		13.6	3.48	0.067
Zn-loaded Ga_2O_3[e]	1473	0.0		11.3	3.47	0.047

[a] Coordination number. [b] Atomic distance. [c] The empirical parameter for the Zn−Zn shell was extracted from the second coordination peak in the spectrum of the ZnO sample. [d] The empirical parameter for the Zn−Ga shell was extracted from the second coordination peak in the spectrum of the $ZnGa_2O_4$ sample. [e] The $Ga_2O_3(K_1)$ sample was used. Loading amount of Zn was 2 mol %. Zn ion was loaded by the impregnation method, followed by calcination at various temperatures for 6 h.

The activities for the WD and the MD were examined for some of the Pt(0.01)/β-Ga_2O_3:M samples in the flow of each reactant. Results are shown in Table 5. The hydrogen production rate in the WD increased in the sample doped with Mg^{2+} (1 mol %) or Al^{3+} (1 mol %) but it decreased in the sample doped with In^{3+} (2 mol %) or Sr^{2+} (2 mol %), which was the same tendency as the activity for the PSRM. On the other hand, the hydrogen production rate in the MD did not increase in all samples. These results show that metal ions doped into the bulk of the β-Ga_2O_3 would contribute to the improvement of water activation.

Loading Effect of Metal Ion. Loading metal oxide particles on the surface of the β-Ga_2O_3 was carried out by the impregna-

TABLE 5: Effect of the Reaction Gas on the Hydrogen Production Rate over the Pt(0.01)/β-Ga_2O_3:M Photocatalysts in the Flow of Various Reactants[a]

	H_2 production rate/μmol min^{-1}		
metal ion	(a) $H_2O + CH_4$	(b) H_2O	(c) CH_4
Mg 1 mol %	0.72	0.30	0.13
Al 1 mol %	0.63	0.17	0.14
bare	0.51	0.15	0.15
In 2 mol %	0.33	0.04	0.05
Sr 2 mol %	0.18	0.11	0.02

[a] The Ga_2O_3(S) sample was used. Pt was loaded by the impregnation method, followed by calcination at 773 K.

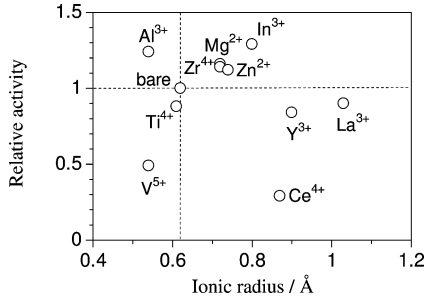

Figure 9. Relative activity of the Pt(0.01)/MO_x(0.1)/β-Ga_2O_3 samples to the Pt(0.01)/β-Ga_2O_3 sample for the PSRM plotted vs ionic radius of each doping metal ion (M). The Ga_2O_3(S) sample was used. Pt was loaded by the impregnation method, followed by calcination at 773 K.

tion method, followed by calcination at 773 K. In this case, the optimum loading amount for the improvement of the photocatalytic activity was found typically to be around 0.1 mol %. The activities of the Pt(0.01)/β-Ga_2O_3 samples loaded with 0.1 mol % of metal ions, Pt(0.01)/MO_x(0.1)/Ga_2O_3, are shown in Figure 9. It is difficult to find clear correlation between the activity and the ionic radius or the oxidation number of metal ions, which was different from the result shown in Figure 5. In other words, the activity of the catalyst calcined at 773 K showed a different tendency from that of the catalyst calcined at 1273 K. This seems reasonable because the state of metal ions would be different between these two series of samples. The addition of Al^{3+}, Zr^{4+}, Mg^{2+}, Zn^{2+}, or In^{3+} increased the photocatalytic activity. These ions would exist as metal oxide particles on the β-Ga_2O_3 surface as analogically suggested from the XAFS analyses on the Mg^{2+}- and Zn^{2+}-loaded samples. The highest activity was obtained over In_2O_3-loaded catalyst, Pt(0.01)/In_2O_3(0.1)/β-Ga_2O_3, which showed 1.3 times higher activity than the Pt(0.01)/β-Ga_2O_3 sample without the addition of metal ions. It could be said that a high activity was obtained when the homologous element of Ga such as In^{3+} and Al^{3+} was added. Although the reason for this result has not been clarified, one possibility is that homologous elements of Ga may be easily dispersed on the surface of the β-Ga_2O_3 and form active sites to increase the activity. On the other hand, the addition of metal ions that may be easily reduced in the presence of methane upon photoirradiation, such as V^{5+}, Ti^{4+}, and Ce^{4+}, largely decreased the photocatalytic activity. Therefore, it was suggested that metal ions without changing their oxidation number would be effective as the surface additives.

The activities for the WD and the MD were examined for some of the Pt(0.01)/MO_x/β-Ga_2O_3 samples in the flow of each reactant. Results are shown in Table 6. The activity for the WD did not increased in all samples. However, the order of the activity for the MD was the same as that of the activity for the

TABLE 6: Effect of the Reaction Gas on the Hydrogen Production Rate over the Pt(0.01)/MO_x(0.1)/β-Ga_2O_3 Photocatalysts in the Flow of Various Reactants[a]

	H_2 production rate/μmol min^{-1}		
metal ion	(a) $H_2O + CH_4$	(b) H_2O	(c) CH_4
In	0.66	0.12	0.17
Al	0.63	0.14	0.16
bare	0.51	0.15	0.15
Y	0.43	0.15	0.14
V	0.25	0.12	0.02

[a] The Ga_2O_3(S) sample was used. Pt was loaded by the impregnation method, followed by calcination at 773 K.

TABLE 7: Effect of Mg Doping and the In_2O_3 Addition on the Hydrogen Production Rate in the PSRM over the Pt(0.01)/β-Ga_2O_3 Photocatalyst[a]

entry	photocatalyst	H_2 production rate/μmol min^{-1}
1	Pt/β-Ga_2O_3	0.41
2	Pt/β-Ga_2O_3:Mg(1)	0.55
3	Pt/In_2O_3(0.05)/β-Ga_2O_3	0.48
4	Pt/In_2O_3(0.05)/β-Ga_2O_3:Mg(1)	0.65

[a] The Ga_2O_3(K_1) sample was used. Pt was loaded by the impregnation method, followed by calcination at 773 K.

PSRM. These suggest that the metal ions that existed on the surface of the β-Ga_2O_3 would contribute to the enhancement of the methane activation. Results of Tables 5 and 6 support our hypotheses mentioned above that the bulk property of the photocatalyst would mainly influence the water activation while the surface property of the photocatalyst would mainly influence the methane activation.

Since the different effects were obtained by the addition of metal ions on the surface and the doping of them into the bulk of β-Ga_2O_3, both modifications were examined at the same time. Mg ion (1 mol %) was added on β-Ga_2O_3, followed by calcination at 1273 K to obtain the doped β-Ga_2O_3:Mg(1) sample. Then, In ion (0.05 mol %) was mounted on the Mg-doped sample, followed by calcination at 773 K to obtain the In_2O_3(0.05)/β-Ga_2O_3:Mg(1) sample. Finally, Pt was deposited on the sample. The photocatalytic activity of this sample was compared with the Pt(0.01)/β-Ga_2O_3, Pt(0.01)/β-Ga_2O_3:Mg(1) and Pt(0.01)/In_2O_3(0.05)/β-Ga_2O_3 samples, as shown in Table 7. As mentioned above, the Pt/β-Ga_2O_3:Mg sample showed 1.3 times higher activity than the Pt/β-Ga_2O_3 sample did (Table 7, entry 2). The activity of the Pt/In_2O_3/β-Ga_2O_3 sample was also 1.2 times higher than that of the Pt/β-Ga_2O_3 sample (Table 7, entry 3). It was found that the activity of the Pt/In_2O_3/β-Ga_2O_3:Mg sample was 1.6 times higher than that of the Pt/β-Ga_2O_3 sample (Table 7, entry 4). The activity of this doubly modified Pt/β-Ga_2O_3 catalyst was also in good agreement with the expected activity based on the assumption that both Mg^{2+} doping and In_2O_3 loading would enhance the activity independently at the same time ($1.2 \times 1.3 = 1.6$). These results suggest that the each modification would improve the bulk property and the surface property, each of which would enhance the activation of water and methane, respectively.

Conclusions

Photocatalytic steam reforming of methane proceeded over Ga_2O_3 around room temperature (ca. 308 K). The activity was largely influenced by the crystal structure and surface area of the Ga_2O_3 samples as well as cocatalyst. In the present study,

the Pt-loaded β-Ga_2O_3 photocatalyst with specific surface area of 10−20 $m^2\ g^{-1}$ was effective for the PSRM without deactivation for a long time.

The β-Ga_2O_3 sample with a large surface area was effective for the methane activation, while the one with a small surface area was effective for the water activation. In other words, the rate for methane activation would be mainly determined by the surface process such as surface reaction or adsorption/desorption, while that for the water activation would be influenced by the bulk process such as migraton of carriers or their recombination probability. The metal cocatalyst influenced the activation of both water and methane, because metal cocatalyst would not only promote the separation of electrons and holes to reduce their recombination but also work as the reaction site on the surface.

The activity of the Pt/β-Ga_2O_3 sample was further enhanced by the addition of metal ions into the bulk and on the surface. As the dopant into the bulk of β-Ga_2O_3, the metal ions with smaller oxidation number having similar ionic radius with that of Ga^{3+}, such as Mg^{2+} and Zn^{2+}, were effective. On the other hand, the homologous elements of Ga^{3+}, such as In^{3+} and Al^{3+}, were most effective as the surface additives. These two kinds of modification could independently improve the activation of water and methane, respectively, at the same time. These factor confirmed that the bulk property of Ga_2O_3 would mainly influence the water activation, while the surface property affected the methane activation, respectively.

Acknowledgment. We thank Dr. L. Yuliati for Ga K-edge XANES analysis of the Ga_2O_3 polymorphs. The X-ray absorption experiments of the Zn-loaded Ga_2O_3 samples were performed under the approval of the Photon Factory Program Advisory Committee (Proposal No. 2008G510). The X-ray absorption experiments of the Mg-loaded Ga_2O_3 samples were performed under the approval of the UVSOR Facility. This work was partially supported by a Grant-in-Aid for Scientific Research on Priority Areas (No. 19028023, "Chemistry of Concerto Catalysis") and for Scientific Research (c) from the Ministry of Education, Culture, Sports, Science and Technology (MEXT) of the Japanese Government. K.S. was supported by a Grant-in-Aid for Nagoya University Global COE programs (Elucidation and Design of Materials and Molecular Functions).

References and Notes

(1) Maeda, K.; Domen, K. *J. Phys. Chem. C* **2007**, *111*, 7851–7861.
(2) Kudo, A.; Miseki, Y. *Chem. Soc. Rev.* **2009**, *38*, 253–278.
(3) Inoue, Y. *Energy Environ. Sci.* **2009**, *2*, 364–386.
(4) Sakata, T.; Kawai, T. *Nature* **1979**, *282*, 283–284.
(5) Kawai, T.; Sakata, T. *Nature* **1980**, *286*, 474–476.
(6) Hashimoto, K.; Kawai, T.; Sakata, T. *J. Phys. Chem.* **1984**, *88*, 4083–4088.
(7) Kawai, T.; Sakata, T. *J. Chem. Soc., Chem. Commun.* **1980**, *15*, 694–695.
(8) Sakata, T.; Kawai, T. *Chem. Phys. Lett.* **1981**, *80*, 341–344.
(9) Sato, S.; White, J. M. *Chem. Phys. Lett.* **1980**, *70*, 131–134.
(10) Sato, S.; White, J. M. *J. Am. Chem. Soc.* **1980**, *102*, 7206–7210.
(11) Yoshida, H.; Kato, S.; Hirao, K.; Nishimoto, J.; Hattori, T. *Chem. Lett.* **2007**, *36*, 430–431.
(12) Yoshida, H.; Hirao, K.; Nishimoto, J.; Shimura, K.; Kato, S.; Itoh, H.; Hattori, T. *J. Phys. Chem. C* **2008**, *112*, 5542–5551.
(13) Shimura, K.; Kato, S.; Yoshida, T.; Itoh, H.; Hattori, T.; Yoshida, H. *J. Phys. Chem. C* **2010**, *114*, 3493–3503.
(14) Shimura, K.; Yoshida, H. *Energy Environ. Sci.* **2010**, *3*, 615−617.
(15) Kato, H.; Asakura, K.; Kudo, A. *J. Am. Chem. Soc.* **2003**, *125*, 3082–3089.
(16) Domen, K.; Naito, S.; Soma, M.; Ohnishi, T.; Tamaru, K. *J. Chem. Soc., Chem. Commun.* **1980**, *12*, 543–544.
(17) Mizoguchi, H.; Ueda, K.; Orita, M.; Moon, S.-C.; Kajihara, K.; Hirano, M.; Hosono, H. *Mater. Res. Bull.* **2002**, *37*, 2401–2406.
(18) Ishihara, T.; Nishiguchi, H.; Fukamachi, K.; Takita, Y. *J. Phys. Chem. B* **1999**, *103*, 1–3.
(19) Kudo, A.; Sayama, K.; Tanaka, A.; Asakura, K.; Domen, K.; Muruya, K.; Onishi, T. *J. Catal.* **1989**, *120*, 337–352.
(20) Yanagida, T.; Sakata, Y.; Imamura, H. *Chem. Lett.* **2004**, *33*, 726–727.
(21) Sakata, Y.; Matsuda, Y.; Yanagida, T.; Hirata, K.; Imamura, H.; Teramura, K. *Catal. Lett.* **2008**, *125*, 22–26.
(22) Yuliati, L.; Hattori, T.; Itoh, H.; Yoshida, H. *J. Catal.* **2008**, *257*, 396–402.
(23) Yuliati, L.; Itoh, H.; Yoshida, H. *Chem. Phys. Lett.* **2008**, *452*, 178–182.
(24) Zheng, B.; Hua, W.; Yue, Y.; Gao, Z. *J. Catal.* **2005**, *232*, 143–151.
(25) Nomura, M.; Koike, Y.; Sato, M.; Koyama, A.; Inada, Y.; Asakura, K. *AIP Conf. Proc.* **2007**, *882*, 896.
(26) Nishi, K.; Shimizu, K.; Takamatsu, M.; Yoshida, H.; Satsuma, A.; Tanaka, T.; Yoshida, S.; Hattori, T. *J. Phys. Chem. B* **1998**, *102*, 10190–10195.
(27) Sato, S.; White, J. M. *Chem. Phys. Lett.* **1980**, *72*, 83–86.
(28) Michaelson, H. B. *J. Appl. Phys.* **1977**, *48*, 4729–4733.
(29) Karakitsou, K. E.; Verykios, X. E. *J. Phys. Chem.* **1993**, *97*, 1184–1189.
(30) Kato, H.; Kudo, A. *Chem. Phys. Lett.* **2000**, *331*, 373–377.
(31) Iwase, A.; Okutomi, H.; Kato, H.; Kudo, A. *Chem. Lett.* **2004**, *10*, 1260–1261.
(32) Arai, N.; Saito, N.; Nishiyama, H.; Inoue, Y.; Domen, K.; Sato, K. *Chem. Lett.* **2006**, *35*, 796–797.
(33) Takata, T.; Domen, K. *J. Phys. Chem. C* **2009**, *113*, 19386–19388.
(34) Ohno, T.; Sarukawa, K.; Tokieda, K.; Matsumura, M. *J. Catal.* **2001**, *203*, 82–86.
(35) Hurum, D. C.; Agrios, A. G.; Gray, K. A.; Rajh, T.; Thurnauer, C. *J. Phys. Chem. B* **2003**, *107*, 4545–4549.
(36) Ikarashi, K.; Sato, J.; Kobayashi, H.; Saito, N.; Nishiyama, H.; Inoue, Y. *J. Phys. Chem. B* **2002**, *106*, 9048–9053.
(37) Moriga, T.; Sakamoto, T.; Sato, Y.; Khalid, A. H.; Suenari, R.; Nakabayashi, I. *J. Solid State Chem.* **1999**, *142*, 206–213.

JP1012126